Journal of Materials Chemistry

Cite this: *J. Mater. Chem.*, 2012, **22**, 13216

www.rsc.org/materials

PAPER

Sulfated mesoporous Au/TiO_2 spheres as a highly active and stable solid acid catalyst†

Cheng Chao Li,[a] Yan Ping Zheng[b] and Tai Hong Wang*[a]

Received 30th December 2011, Accepted 20th April 2012
DOI: 10.1039/c2jm16921e

In this work, we reported several kinds of highly stable, effective mesoporous Au/TiO_2 sphere-based solid acid catalysts with large specific surface areas and good monodispersity in the reaction medium. In this process, monodisperse titanium glycolate spheres were first formed by an antisolvent precipitation route, and were then converted to mesoporous TiO_2 by *in situ* hydrolysis under hydrothermal conditions. The resultant uniform TiO_2 spheres were subsequently functionalized with sulfate anions at different temperatures or incorporated with tungstophosphoric acid (TPA); the solid acid catalysts were thus fabricated. In particular, our monodisperse spherical catalysts with large specific surface area have shown remarkable performance in a wide range of acid-catalyzed reactions such as Friedel–Crafts alkylation, esterification and hydrolysis of acetate. The TiO_2-based catalysts could be separated and reused showing no deactivation.

Introduction

Heterogeneous acid catalysts (*e.g.* $AlCl_3$, BF_3, HCl, and H_2SO_4), a very important class of catalysts, are commonly used in many industrially important reactions such Friedel–Crafts alkylation, esterification, and hydrolysis.[1–8] However, major drawbacks of these catalysts include separation and recovery from the reaction solution, corrosion, high toxicity, and disposal of spent catalyst, *etc.*[8–17] Besides, some of the catalysts are very moisture sensitive, which increases the difficulty of reaction operation and requires high-level reaction equipment. Thus, development of reusable solid catalysts with high activity and low cost is of great practical importance. In comparison with the liquid acid catalysts, solid acid catalysts are environmentally friendly with regard to corrosiveness and safety, and readily separable from the reaction system. Intrigued by this, increasing research interest has focused on the substitution of hazardous Lewis and Brønsted acid catalysts by heterogeneous analogues. To date, silica-supported solid acid catalysts, styrene-based sulfonic acid resins, sulfonated mesoporous carbon, zeolites and heteropolyacids, and metal oxides have been developed and investigated as solid acid catalysts.[18–30] However, their heterogeneous nature does not guarantee the stability of catalytic performance after their recovery because polymerization of the neat reactants may have occurred over the course of the reaction, resulting in coverage of active sites. In addition, the use of toxic organic ligands and solvents in the synthesis of these solid acid catalysts is still a crucial issue. Recently, molybdenum oxides have been demonstrated as a highly effective solid acid catalyst in benzylation of a broad range of arenes with various benzylic alcohols as alkylating agents.[31–33] However, despite their good catalytic performance, the practical use of MoO_3 as a solid acid catalyst is still largely hindered by the high cost and large scale synthesis. Despite recent advances, there is still a demand for other low cost and environmentally friendly solid acid alternatives. Titanium oxide and titanium-containing catalysts have recently attracted great interest due to their high stability and strong acid properties which can be preserved in polar liquids.[34–39] Furthermore, titanium is the second most abundant transition metal in the earth's crust. In view of catalytic reactions, it is known that the catalytic activity of a solid acid catalyst is greatly dependent on the chemical active sites and diffusion rate of reaction substrate. For this reason, nanostructured or/and porous titanium oxide catalysts with large surface area hold much promise for the development of solid acid catalysts with enhanced activity. The short diffusion channels and large surface area in theory allow more facile diffusion of the reaction substrate compared to bulk materials, and thus a higher reaction rate is achieved. In pursuing this research, there have been a number of synthetic methods proposed in recent years, such as solvent–thermal/hydrothermal routes, template routes, electrospinning, sol–gel, and so on.[40–44] In addition to these methods, in the present study, we develop a novel *in situ* hydrolysis approach to synthesize monodisperse mesoporous Au/TiO_2 spheres and their solid acid catalyst derivatives. In the synthesis, acetone acts as an antisolvent. When

[a]*Key Laboratory for Micro-Nano Optoelectronic Devices of Ministry of Education, State Key Laboratory of Chemo/Biosensing and Chemometrics, Hunan University, Changsha, 410082, P. R. China. E-mail: thwang@aphy.iphy.ac.cn; Fax: +86-0731-88822137; Tel: +86-0731-88823407*
[b]*State Key Laboratory of Physical Chemistry of Solid Surfaces, College of Chemistry and Chemical Engineering, Xiamen University, Xiamen, 361005, China*
† Electronic supplementary information (ESI) available. See DOI: 10.1039/c2jm16921e

the solvent containing titanium precursors is poured into acetone, titanium glycolate segregates from the mixed solvents to form the spherical product due to large supersaturation with the assistance of water.[45–48] The obtained mesoporous Au/TiO_2 in our work can be easily functionalized with sulfate anions at different temperatures or incorporated with tungstophosphoric acid (TPA) to obtain a series of recyclable solid acid catalysts. Thanks to their large surface area and short diffusion channels, the prepared catalysts exhibit superior catalytic activities for Friedel–Crafts alkylation, esterification, and hydrolysis of acetates. In particular, the catalysts still maintained a similar catalytic performance to the fresh one after using eight times.

Experimental section

The sulfated mesoporous Au/TiO_2 spheres were prepared by a three-step route: (i) synthesis of titanium glycolate precursor spheres; (ii) hydrolysis of the titanium glycolate spheres to fabricate mesoporous Au/TiO_2 spheres; and (iii) treatment of Au/TiO_2 spheres by sulfuric acid and TPA.

Synthesis of titanium glycolate precursor spheres

All chemicals were available commercially and used without further purification. The titanium glycolate spheres were synthesized according to the route reported previously with minor modification.[44] In a typical synthesis, tetrabutoxytitanium (TBT, Aldrich) was added to ethylene glycol (EG, 50 mL, Merck) in a 100 mL flask under vigorous stirring; then nitrogen was bubbled through the system for about 30 min to remove water and oxygen. After that, the flask was sealed and stirred for 12 h at room temperature. The obtained mixture was poured into 200 mL acetone in a beaker, followed by the addition of 1.9 mL water and 0.8 mL 30 mM $HAuCl_4$. The beaker was then sealed with Parafilm and stirred for 1 h. The white precipitate was harvested by centrifugation, washed with ethanol three times and dried at 50 °C in an oven for further usage.

Synthesis of mesoporous Au/TiO_2 spheres

0.5 g titanium glycolate precursor spheres were dispersed into 40 mL water under the assistance of ultrasonication. The mixture was then transferred to a Teflon-lined autoclave and kept inside an electric oven at 180 °C for 4 h. The product was collected, washed several times with water and ethanol, and then dried at 60 °C in an oven.

Catalysts preparation

Sulfated mesoporous titanium oxide. The obtained mesoporous titanium oxide spheres were dispersed in 20 mL methanol solution containing 1 M sulfuric acid under vigorous stirring for 6 h. The obtained product was collected by centrifugation and calcined at 100 °C or 400 °C for 4 h to obtain the sulfated titanium oxide.

Sulfated titanium oxide particles. The titania particles purchased from Merck were sulfated using the same route as our mesoporous titanium oxide spheres.

Characterization

Crystallographic phases of the prepared products were investigated by X-ray power diffraction method (XRD) using Shimadzu XRD-6000 with Cu Kα radiation. The morphologies of the as-prepared samples were characterized by field-emission scanning electron microscopy (FESEM; JSM-6700F), transmission electron microscopy (TEM; JEM-2010, 200 kV), selected area electron diffraction (SAED), and high-resolution transmission electron microscopy (HRTEM; JEM-3010, 300 kV). The Fourier transform infrared (FTIR) spectrum was recorded for a KBr dilute sample using a Bio-Rad FTS-135 FTIR spectrometer. Thermogravimetric analysis (TGA; Shimadzu TGA-50) was also performed to determine the composition of the sample. The TGA measurements were carried out at a heating rate of 10 °C min^{-1} from 50 °C to 900 °C with an air flow rate of 100 mL min^{-1}. Specific surface area measurement and porosity analysis for the titanium oxide spheres samples were performed using N_2 adsorption–desorption isotherms (Quantachrome NOVA-3000 system at 77 K). NH_3-TPD was carried out using a Micromeritics Auto Chem II 2920 instrument equipped with a Pfeiffer Vacuum ThermoStar GSD 301 T2 mass spectrometer. After the sample was heated at 373 K for 2 h under He flow, a certain amount of the sample was exposed to NH_3 at 353 K for adsorption and then heated at 10 K min^{-1}. Slightly compacted ground sulfated TiO_2 was previously heated up to 100 °C for 30 min in a catalytic cell. After this period of time, pyridine vapor was introduced into the cell, the inlet valve was left open for 3 min, after which a vacuum was produced in order to remove excess pyridine. The infrared spectra were then acquired at 200 °C.

Catalytic tests

The catalytic reaction of mesoporous titanium oxide spheres was carried out in a 100 mL 3-neck-round bottom flask with a reflux condenser. 50 mL of toluene, 5 mL of benzyl alcohol and 0.5 mL internal standard hexadecane were added to the reactor with 0.5 g catalyst in each run. Nitrogen was introduced into the flask through one of the gas inlets. The second inlet was equipped with a septum for sample removal. The reaction mixture was heated to 130 °C for a certain time using an oil bath. Samples of the reaction mixture were periodically withdrawn from the flask and analyzed by gas chromatography (GC). The temperature was programmed from 70 °C to 280 °C. The results from GC identify the *o*- and *p*-benzylation products and benzyl ether as the main products of these reactions. Activities were calculated on the basis of percentage conversion of benzyl alcohol in the starting mixture.

Catalyst recycling and reuse

The catalyst was separated from the reaction mixture by centrifugation, and then rinsed with toluene three times. The collected catalyst was directly dispersed into the fresh reaction mixture (5 mL benzyl alcohol and 50 mL toluene) to conduct the next recycling test. In all reuse tests, the sampling time was 40 min for convenience.

Results and discussion

Fig. 1 depicts the synthetic steps for the sulfated mesoporous Au/TiO_2 spheres solid acid catalysts prepared in this work. First, tetrabutoxytitanium was dissolved in ethylene glycol and reacted with ethylene glycol to form glycolate derivatives according to eqn (1) and (2).[44,49–51]

$$Ti(OBu)_4 + HOCH_2CH_2OH \rightarrow Ti(OCH_2CH_2O)(OBu)_2 + 2HOBu \quad (1)$$

$$Ti(OBu)_4 + HOCH_2CH_2OH \rightarrow Ti(OCH_2CH_2O)_2 + 4HOBu \quad (2)$$

Due to their low solubility in acetone, glycolate derivatives segregate when poured into acetone. At the same time, $AuCl_4^-$ adsorbs on the surface of these spheres and makes them more stable against aggregation by increasing their surface potential. The morphology of the obtained titanium glycolate spheres was investigated by transmission electron microscopy (TEM). As depicted in Fig. 2a, it reveals the products are uniform and spherical with sizes around 500 nm. By hydrothermal treatment at 180 °C, titanium glycolate spheres were converted to mesoporous titanium oxide spheres by *in situ* hydrolysis. From the SEM images (Fig. 2b), the spherical morphology was completely preserved and the surface of the spherical particles became very rough. The TEM images further reveal the porous nature of the materials, as shown in Fig. 2c and d. The pores in mesoporous spheres (several nanometers) are clearly observed. The mesoporous spheres are composed of a lot of interconnected nanoparticles with sizes around 10 nm, which is compatible with results calculated by Scherrer's equation. During the hydrothermal process, the $AuCl_4^-$ adsorbed on the surface of the spheres was also reduced into gold nanoparticles (Fig. 2d). The dynamic light scattering (DLS) results (Fig. 2f) show that the average hydrodynamic diameters of the spheres are about 500 ± 50 nm, which is consistent with the SEM results. The phase

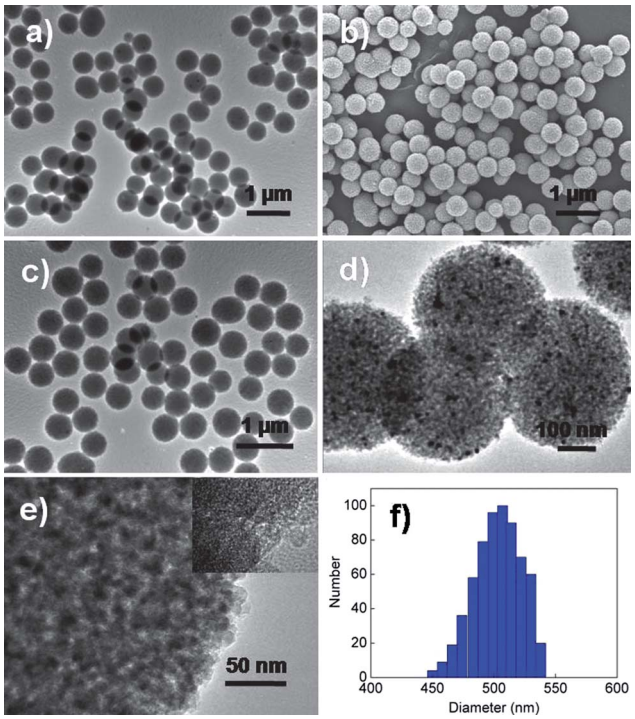

Fig. 2 (a) The representative TEM images of titanium glycolate spheres, (b) SEM images and (c–e) TEM of the as-prepared mesoporous titanium oxide spheres (MTOS), (f) DLS size-distribution diagram of MTOS.

structure of the as-synthesized samples was characterized using power X-ray diffraction (XRD). Fig. 3 shows a representative diffraction pattern. All these peaks can be indexed to the pure anatase structure of TiO_2. The lattice parameter *a* is found to be 0.378 nm by analysis of the XRD pattern, which is in agreement with the reported values (JCPDS card no. 21-1272). Compared with those of the bulk counterpart, the peaks are relatively broadened, which demonstrates the small size of the nanoparticles. No characteristic peaks of other impurities are

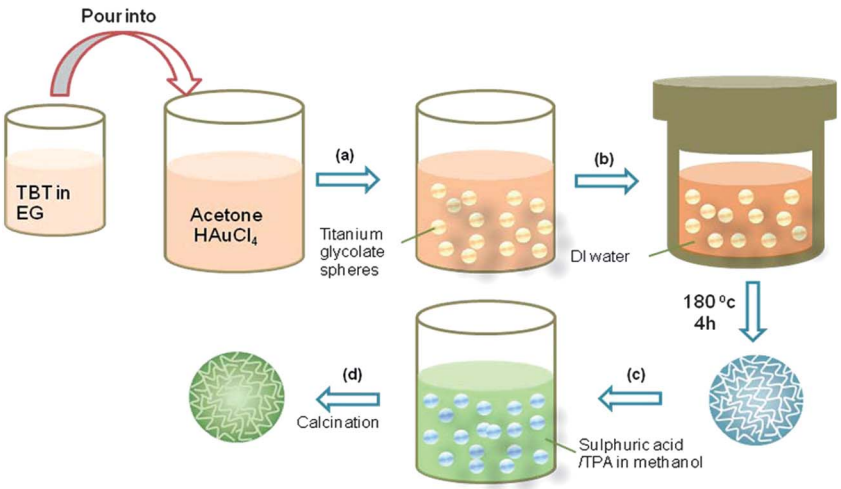

Fig. 1 Typical preparation process of sulfated mesoporous Au/TiO_2 spheres solid acid catalysts: (a) mixing EG (solvent) containing TBT and acetone (antisolvent), (b) hydrothermal treatment of titanium glycolate spheres, (c) functionalization with sulfate groups or TPA, (d) calcination at different temperatures.

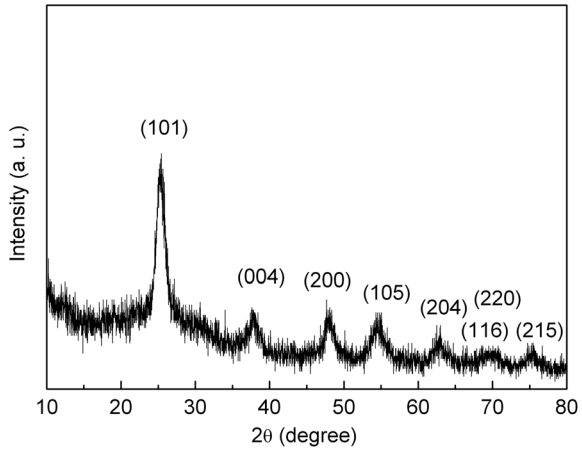

Fig. 3 XRD pattern of as-prepared mesoporous Au/TiO_2 spheres.

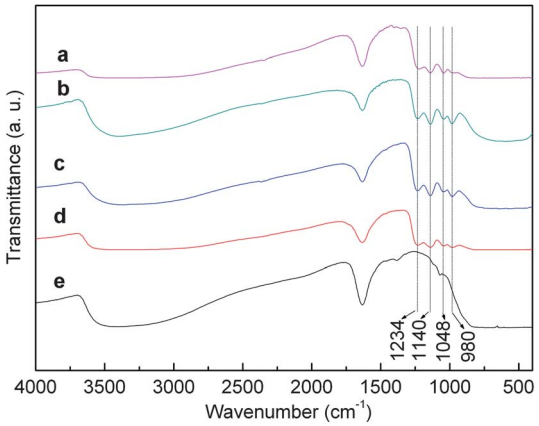

Fig. 5 FTIR spectra of the sulfated MTOS catalysts after various heat treatments: (a) at 100 °C, (b) at 200 °C, (c) at 300 °C, (d) at 400 °C for 4 h and (e) non-sulfated MTOS for reference.

observed, indicating the purity of the product. In order to estimate the surface areas, the mean diameters and volumes of the pores, nitrogen adsorption–desorption measurements at 77 K have been carried out. Fig. 4 presents the isotherm of the Au/TiO_2 spheres and its corresponding pore size distribution curve. The isotherm can be classified as type IV isotherm, characteristic of mesoporous materials. The corresponding pore size distribution calculated from the isotherm by the Barrett–Joyner–Halenda (BJH) method shows a narrow pore size distribution ranging from 2 nm to 8 nm. The Brunauer–Emmett–Teller (BET) surface area and pore volume are 153.3 $m^2\ g^{-1}$ and 0.3 $cm^3\ g^{-1}$, respectively.

The as-prepared mesoporous Au/TiO_2 spheres were treated by sulfuric acid or tungstophosphoric acid (TPA) at different temperatures to obtain the solid acid catalysts. There are three states—simple coordination, chelation coordination and bridge coordination—for the sulfate moiety existing on the surface of TiO_2. The bonding situations of sulfated species are revealed by the FTIR spectrum (Fig. 5). The band at 1625 cm^{-1} is assigned to the deformation vibration mode of the adsorbed water. In comparison with TiO_2, new absorption bands between 1250 and 950 cm^{-1} are observed in all sulfated MTOS catalysts, and are assigned to a bidentate sulfate ion coordinated to the Ti atoms.[52–54] These bands are related to the amount of sulfate linked to the metal oxide in the chelate form. The bands at 1234 and 1140 cm^{-1} can be attributed to the asymmetric and symmetric stretching vibrations of S=O groups, respectively, while the peaks centered at 1048 cm^{-1} are ascribed to asymmetric stretching vibrations of S–O groups. For mesoporous Au/TiO_2 calcined at 400 °C, the band intensities of the sulfate ion decrease slightly because of the partial decomposition of sulfate ions.

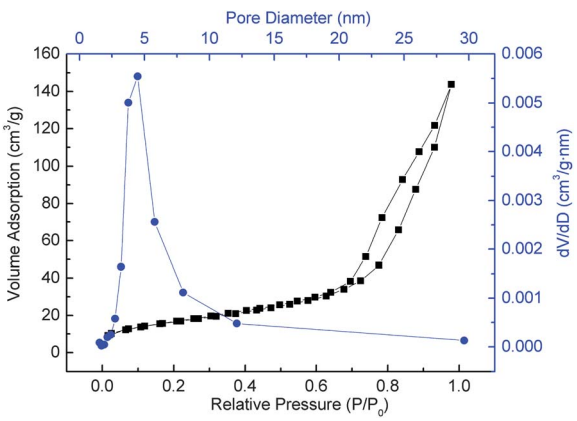

Fig. 4 N_2 adsorption–desorption BET isotherm and pore size distribution curve.

The surface element composition and chemical state of the sample were further confirmed by XPS results, and the corresponding experimental results are shown in Fig. 6. The Ti 2p XPS spectrum shows two major peaks with binding energies at 464.9 eV and 459.1 eV, corresponding to Ti $2p_{3/2}$ and Ti $2p_{1/2}$, respectively, characteristic of a TiO_2 phase. Fig. 6b is an XPS spectrum of S, which confirms the existence of SO_4^{2-}. It can be fitted into two peaks (S $2p_{3/2}$ and a S $2p_{1/2}$ doublet) by nearly Gaussian curves. The spectrum of O 1s with an additional shoulder at higher binding energy is observed and can be fitted into three peaks. The lower energy peak located at 530.4 eV corresponds to the coordination of oxygen in Ti–O–Ti, while the higher energy peak centered at 531.9 eV can be ascribed to the O–S binding. Another small peak located at 533.1 eV should be assigned to OH species in H_2O molecules. The XPS peaks of 86.4 and 81.2 eV with a constant separation of spin orbit coupling of 5.2 eV are clearly observed, which correspond to Au $4f_{7/2}$ and $4f_{5/2}$, respectively.

Further, NH_3 temperature-programmed desorption (NH_3-TPD) experiments have been carried out to investigate the acidity of these solid acid catalysts based on MTOS (Fig. SI-1†). As we know, sulfate species themselves are Lewis acids and they can generate Lewis and Brønsted acidity centers by adsorption on the metal oxide surfaces. Also, Lewis and Brønsted sites on the metal oxide surfaces are easily changeable by adsorption or desorption of water molecules. The chemical state of the sulfate groups sometimes determines the acidity of the oxide surfaces. Generally, the ionic character between a metal center and sulfate anions is changed to covalent character after calcination at high temperature, which is responsible for generating strongly acidic active centers on the oxide surfaces. It is proposed that sulfate species are combined with Ti elements in the bridging bidentate

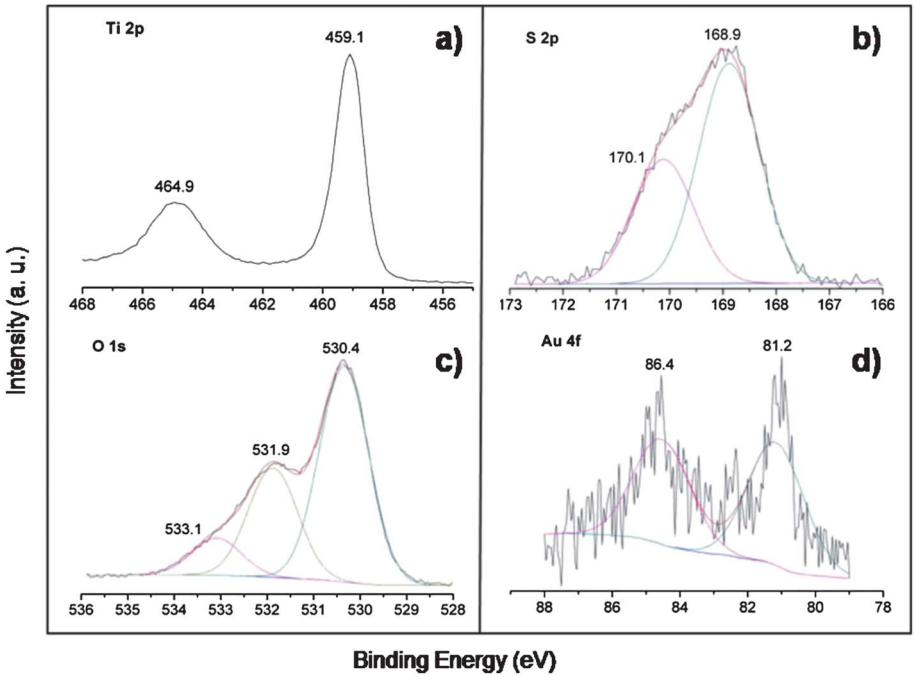

Fig. 6 XPS survey spectra of mesoporous Au/TiO_2 spheres: (a) Ti 2p, (b) S 2p, (c) O 1s, (d) Au 4f.

state.[55] The double-bond nature of the complex (Ti–OOSOO–Ti) is much stronger compared to that of a simple metal sulfate (Fig. SI-2†). Due to the electron-withdrawing effect of SO_4^{2-}, the Lewis acid strength of Ti^{4+} would be remarkably stronger. For TPD analysis, the peak temperature is a measure of the strength of acid sites while the area under the peak represents the total amount of acid sites present on the catalyst. The NH_3-TPD profile of sulfated MTOS at 100–400 °C shows a wide NH_3 desorption band ranging from 100 to 400 °C, which can be considered an indication of the presence of a high concentration of acid sites with moderate strength. In addition to this broad peak, a shoulder peak above 420 °C was also observed for sulfated MTOS at 300 and 400 °C. The formation of superacid sites could be responsible for the presence of the high-temperature desorption peaks, which is in agreement with literature reports. It should be noted that the peak intensity for sulfated MTOS at 400 °C is much weaker than that of sulfated MTOS at 300 °C. This can be related to the partial decomposition of the sulfate ion, which is consistent with FTIR results. To detect the presence of Lewis and Brønsted acid sites on the catalysts, as well as their acid strength, pyridine adsorption analysis was carried out in this study. The pyridine adsorption experiments were performed by acquisition of infrared spectra at 200 °C. The corresponding FT-IR spectra of pyridine adsorption are shown in Fig. SI-3.† The spectra show bands of absorption at 1640, 1607, 1538, 1487 and 1445 cm^{-1}, typical of adsorbed pyridine. The bands around 1640 cm^{-1} and 1538 cm^{-1} were attributed to the pyridinium ion (Brønsted acid sites), and bands at about 1607 cm^{-1}, 1487 cm^{-1} and 1445 cm^{-1} were ascribed to coordinated pyridine (Lewis acid sites). The ratio between the Brønsted and Lewis acid sites can be determined from the relative intensity (band heights) of the bands located at 1538 cm^{-1} and 1445 cm^{-1}, related to Brønsted and Lewis acid sites respectively. In agreement with TPD results, the catalysts treated at 200 and 300 °C contain the maximum number of acid sites. However, for the catalyst treated at 400 °C, the intensities of absorption bands assigned to Brønsted acidity (1640 and 1538 cm^{-1}) decrease, indicating that Brønsted acidity will be largely destroyed at higher calcination temperature. As we know, Brønsted acidity is due to free surface hydroxyl groups located near active sulfate species such that the electron-withdrawing effect of the active sulfate species makes proton donation easier. Therefore, the content of active sulfate species on the catalyst surface plays a very important role in the generation of Brønsted acidity. A certain minimum threshold of active sulfate species is required to generate strong Brønsted acidity.

The catalytic activities of these solid acid catalysts based on Au/TiO_2 spheres were evaluated in the benzylation of toluene with benzyl alcohol in liquid phase at a temperature of 130 °C. In order to illustrate the excellent diffusion advantages inherited from the mesoporous sphere structure, nonporous sulfated titanium oxide particles were also tested for comparison. As shown in Fig. 7, the titanium oxide particles show very low catalytic activity in this Friedel–Crafts alkylation reaction: the conversion of alcohol is only 3.12% in 8 h. The pure MTOS shows moderate performance as a catalyst. The TPA/MTOS has a higher catalytic activity than pure MTOS; it shows 100% conversion in less than 8 h. However, the catalytic activity decreases with time. Out of the four catalysts, the best catalytic activity was achieved by the sulfated MTOS treated at 300 °C. The conversion of benzyl alcohol in 30 min is up to 100%. Compared to the solid acid catalyst reported previously, our sulfated MTOS treated at 300 °C also shows much better catalytic performance. The high catalytic performance demonstrates that nanosized porous particles are very effective for heterogeneous catalytic reactions. In our work, the ultrahigh catalytic activity of sulfated MTOS

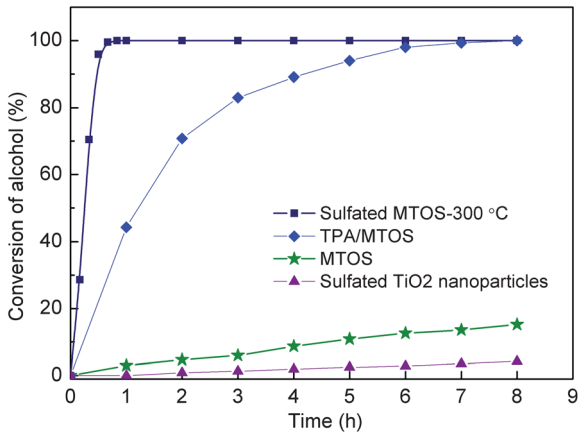

Fig. 7 Percentage conversion of benzyl alcohol in the benzylation of toluene catalyzed by various catalysts.

can be attributed to two advantages: (i) the monodisperse and mesoporous spherical structure; the short diffusion path and large surface area facilitate the diffusion of reactants and products, greatly increasing the reaction rate; (ii) high percentage of sulfate groups covalently immobilized on titanium oxide, increasing the acidity level of MTOS. The heat treatment temperature of sulfated MTOS is a key parameter to catalytic activity, which greatly affects the amount of sulfate groups covalently immobilized on MTOS. The suitable heat treatment temperature ranges from 200 to 300 °C (Fig. SI-4†). When the temperature is above 300 °C, some of the sulfate groups will decompose. However, if the temperature is too low (<200 °C) the percentage of covalently immobilized sulfate groups decreases. After a catalytic reaction, the sulfated MTOS catalyst was easily separated by centrifugation and washed with toluene, and could be used several times. Eight test recycles were performed to evaluate the reusability of sulfated MTOS, as shown in Fig. 8. The reused sulfated MTOS still retained high catalytic performance similar to that of the fresh catalyst; no decrease in catalytic activity was observed after eight uses.

The mesoporous TiO_2 spheres-based solid acid catalysts were also applied for the esterification of acetic acid with ethanol and the hydrolysis of ethyl acetate. The sulfated MTOS also show

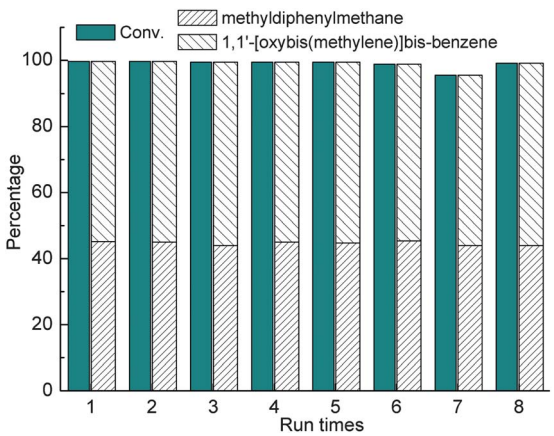

Fig. 8 The reusability of the sulfated MTOS treated at 300 °C.

a high activity for the esterification of acetic acid. The sulfated MTOS treated at 200–300 °C exhibits the highest reaction rate of all the catalysts, achieving a reaction rate of 1.35 mmol g^{-1} min^{-1}. The catalytic activity substantially exceeds the performance of most conventional solid acid catalysts, such as Amberlyst-15, H-Beta, Nafion NR50, and other catalysts reported previously.[32,56] In the hydrolysis of ethyl acetate, interestingly, all the sulfated MTOS show comparable catalytic activity. The reaction rates of sulfated MTOS treated at 100, 200, 300, and 400 °C are 0.28, 0.32, 0.32, and 0.30 mmol g^{-1} min^{-1}, respectively.

Conclusion

In summary, we developed a series of highly stable, effective mesoporous Au/TiO_2 sphere-based solid acid catalysts with large specific surface area and good monodispersity by a three-step route. First, titanium glycolate spheres were prepared and then converted into mesoporous Au/TiO_2 spheres by hydrothermal reaction. Subsequently, Au/TiO_2 spheres were functionalized with sulfate anions at different temperatures or incorporated with tungstophosphoric acid (TPA) to fabricate solid acid catalysts. Due to the large surface area and short diffusion channels, the prepared catalyst exhibited superior catalytic activity for Friedel–Crafts alkylation, esterification and hydrolysis of acetates. In particular, the catalyst still maintained a similar catalytic performance to the fresh one after using eight times.

Acknowledgements

This work was partly supported by the Scholarship Award for Excellent Doctoral Student granted by Ministry of Education (2010), "973" National Key Basic Research Program of China (Grant no. 2007CB310500), National Natural Science Foundation of China (Grant no. 21003041, 21103046), and Hunan Provincial Natural Science Foundation of China (Grant no.10JJ1011).

References

1 G. A. Olah, *Friedel–Crafts Chemistry*, Wiley, New York, 1973.
2 G. A. Olah, G. K. S. J. Prakash and J. Sommer, *Superacids*, Wiley/Interscience, New York, 1985.
3 J. H. Clark, S. R. Cullen, S. J. Barlow and T. W. Bastock, *J. Chem. Soc., Perkin Trans. 1*, 1994, 1117.
4 J. Cao, N. He, C. Li, J. Dong and Q. Xu, *Mesopor. Mol. Sieves*, 1998, **117**, 461.
5 M. Noji, Y. Konno and K. Ishii, *J. Org. Chem.*, 2007, **72**, 5161.
6 J. Liu, Q. Yang, M. P. Kapoor, N. Setoyama, S. Inagaki, J. Yang and L. Zhang, *J. Phys. Chem. B*, 2005, **109**, 12250.
7 I. K. Mbaraka, D. R. Radu, V. S.-Y. Lin and B. H. Shanks, *J. Catal.*, 2003, **219**, 329.
8 X. Wang, C. Chen, S. Chen, Y. Mou and S. Cheng, *Appl. Catal., A*, 2005, **281**, 47.
9 J. A. Melero, J. Iglesias and G. Morales, *Green Chem.*, 2009, **11**, 1285.
10 M. Gruttadauria, F. Giacalone and R. Noto, *Chem. Soc. Rev.*, 2008, **37**, 1666.
11 S. Dasgupta and B. Tçrçk, *Curr. Org. Synth.*, 2008, **5**, 321.
12 M. Benaglia, A. Puglisi and F. Cozzi, *Chem. Rev.*, 2003, **103**, 3401.
13 G. Sartori and R. Maggi, *Chem. Rev.*, 2006, **106**, 1077.
14 A. A. Kiss, A. C. Dimian and G. Rothenberg, *Adv. Synth. Catal.*, 2006, **348**, 75.
15 F. Figueras, M. Lakshmi Kantam and B. Manoranjan Choudary, *Curr. Org. Chem.*, 2006, **10**, 1627.
16 K. Wilson and J. H. Clark, *Pure Appl. Chem.*, 2000, **72**, 1313.
17 B. Das and N. Chowdhury, *J. Mol. Catal. A: Chem.*, 2007, **263**, 212.

18 H. Hagiwara, M. Sekifuji, T. Hoshi, T. Suzuki, B. Quanxi, K. Qiao and C. Yokoyama, *Synlett*, 2008, 608.
19 B. Das, N. Chowdhury, K. Damodar and K. R. Reddy, *Helv. Chim. Acta*, 2007, **90**, 340.
20 Y. Gu, C. Ogawa, J. Kobayashi, Y. Mori and S. Kobayashi, *Angew. Chem., Int. Ed.*, 2006, **118**, 7375.
21 G. Bartoli, M. Bartolacci, M. Bosco, G. Foglia, A. Giuliani, E. Marcantoni, L. Sambri and E. Torregiani, *J. Org. Chem.*, 2003, **68**, 4594.
22 K. Nakajima, I. Tomita, M. Hara, S. Hayashi, K. Domen and J. N. Kondo, *Adv. Mater.*, 2005, **17**, 1839.
23 M. Rueping, B. J. Nachtsheim and W. Ieawsuwan, *Adv. Synth. Catal.*, 2006, **348**, 1033.
24 K. Mertins, I. Iovel, J. Kischel, A. Zapf and M. Beller, *Angew. Chem., Int. Ed.*, 2005, **44**, 238.
25 K. Motokura, N. Nakagiri, T. Mizugaki, K. Ebitani and K. Kaneda, *J. Org. Chem.*, 2007, **72**, 6006.
26 B. M. Devassy, G. V. Shanbhag, F. Lefebvre, W. Bohringer, J. Fletcher and S. B. Halligudi, *J. Mol. Catal. A: Chem.*, 2005, **230**, 113.
27 D. G. Barton, S. L. Soled, G. D. Meitzner, G. A. Fuentes and E. Iglesia, *J. Catal.*, 1999, **181**, 57.
28 M. Hara, T. Yoshida, A. Takagaki, T. Takata, J. N. Kondo, S. Hayashi and K. Domen, *Angew. Chem., Int. Ed.*, 2004, **43**, 2955.
29 B. M. Choudary, R. S. Mulukutla and K. J. Klabunde, *J. Am. Chem. Soc.*, 2003, **125**, 2020.
30 K. Yamashita, M. Hirano, K. Okumura and M. Niwa, *Catal. Today*, 2006, **118**, 385.
31 X. Wang, H. Wang, Y. Liu, F. Liu, Y. Yu and H. He, *J. Catal.*, 2011, **279**, 301.
32 F. Wang and W. Ueda, *Chem. Commun.*, 2008, 3196.
33 F. Wang and W. Ueda, *Chem.–Eur. J.*, 2009, **15**, 742.
34 R. M. Almeida, L. K. Noda, N. S. Goncalves, S. M. P. Meneghetti and M. R. Meneghetti, *Appl. Catal., A*, 2008, **347**, 100.
35 A. P. Kulkarni and D. S. Muggli, *Appl. Catal., A*, 2006, **302**, 274.
36 Q. Yang, C. Xie, Z. Xu, Z. Gao and Y. Du, *J. Phys. Chem. B*, 2005, **109**, 5554.
37 S. N. A. Jenie, D. S. Kusuma, A. Kristiani, J. A. Laksmono and S. Tursiloadi, *Int. J. Basic Appl. Sci.*, 2010, **10**, 6.
38 M. Hosseini-Sarvari, E. Sodagar and M. M. Doroodmand, *J. Org. Chem.*, 2011, **76**, 2853.
39 M. L. Kantam, S. Laha, J. Yadav, B. M. Choudary and B. Sreedhara, *Adv. Synth. Catal.*, 2006, **348**, 867.
40 Z. Zheng, B. Huang, X. Qin, X. Zhang, Y. Dai, M. Jiang, P. Wang and M. Whangbo, *Chem.–Eur. J.*, 2009, **15**, 12576.
41 E. Formo, E. Lee, D. Campbell and Y. Xia, *Nano Lett.*, 2008, **8**, 668.
42 X. Han, Q. Kuang, M. Jin, Z. Xie and L. Zheng, *J. Am. Chem. Soc.*, 2009, **131**, 3152.
43 H. G. Yang, G. Liu, S. Z. Qiao, C. H. Sun, Y. G. Jin, S. C. Smith, J. Zou, H. M. Cheng and G. Q. Lu, *J. Am. Chem. Soc.*, 2009, **131**, 4078.
44 X. Jiang, T. Herricks and Y. Xia, *Adv. Mater.*, 2008, **15**, 1205.
45 Z. R. Tang, C. D. Jones, J. K. W. Aldridge, T. E. Davies, J. K. Bartley, A. F. Carley, S. H. Taylor, M. Allix, C. Dickinson, M. J. Rosseinsky, J. B. Claridge, Z. Xu, M. J. Crudace and G. J. Hutchings, *ChemCatChem*, 2009, **1**, 247.
46 J. Y. Dong, Y. J. Hsu, D. S. H. Wong and S. Y. Lu, *J. Phys. Chem. C*, 2010, **114**, 8867.
47 M. Kitamura and S. Hironaka, *Cryst. Growth Des.*, 2006, **6**, 1214.
48 M. E. Matteucci, M. A. Hotze, K. P. Johnston and R. O. Williams III, *Langmuir*, 2006, **22**, 8951.
49 R. C. Mehrotra, PhD thesis, London University, 1952.
50 D. M. Puri, PhD thesis, University of Gorakhpur, 1962.
51 D. M. Puri and R. C. Mehrotra, *Indian J. Chem.*, 1967, **51**, 448.
52 A. Corma, *Chem. Rev.*, 1995, **95**, 559.
53 K. Nakamoto, *Infrared and Raman Spectra of Inorganic and Coordination Compounds*, John Wiley & Sons, New York, 1986.
54 T. Yamaguchi, *Appl. Catal.*, 1990, **61**, 1.
55 K. Arata, *Adv. Catal.*, 1990, **37**, 165.
56 C. Tagusagawa, A. Takagaki, A. Iguchi, K. Takanabe, J. N. Kondo, K. Ebitani, S. Hayashi, T. Tatsumi and K. Domen, *Angew. Chem., Int. Ed.*, 2009, **48**, 1128.

